Lab on a Chip

Accepted Manuscript

ROYAL SOCIETY OF CHEMISTRY

www.rsc.org/loc

Lab on a Chip

RSCPublishing

ARTICLE

A MULTIPLE-CHANNEL, MULTIPLE-ASSAY PLATFORM FOR CHARACTERIZATION OF FULL-RANGE SHEAR STRESS EFFECTS ON VASCULAR ENDOTHELIAL CELLS

Cite this: DOI: 10.1039/x0xx00000x

Received 00th January 2013,
Accepted 00th January 2013

DOI: 10.1039/x0xx00000x

www.rsc.org/

R. Booth[a], S. Noh[b] and H. Kim[c]

Vascular endothelial cells (VECs), which line blood vessels and are key to understanding pathologies and treatments of various diseases, experience highly variable wall shear stress (WSS) *in vivo* (1-60dyn/cm^2), imposing numerous effects on physiological and morphological functions. Previous flow-based systems for studying these effects have been limited in range, and comprehensive information on VEC functions at the full spectrum of WSS has not been available yet. To allow rapid characterization of WSS effects, we developed the first multiple channel microfluidic platform that enables a wide range (~x15) of homogeneous WSS conditions while simultaneously allowing trans-monolayer assays, such as permeability and trans-endothelial electrical resistance (TEER), as well as cell morphometry and protein expression. Flow velocity/WSS distributions between channels were predicted with COMSOL simulation and verified by measurement with an integrated micro-flow sensor array. Biomechanical responses of the brain microvascular endothelial cell line bEnd.3 to the full natural spectrum of WSS were investigated with the platform. Under increasing WSS conditions ranging from 0-86 dyn/cm^2, (1) permeabilities of FITC-conjugated dextran and propidium iodide decreased respectively at rates of 4.06e^{-8} and 6.04e^{-8}cm/s per dyn/cm^2; (2) TEER increased at a rate of 0.8 Ωcm^2 per dyn/cm^2; (3) cells increased alignment along the flow direction under increasing WSS; and finally (4) increased protein expression of both tight junction component ZO-1 (~5x) and efflux transporter Pgp (~6x) were observed at 86 dyn/cm^2 compared to static controls via western blot. We conclude that the presented microfluidic platform is a valid approach for comprehensively assaying cell responses to fluidic WSS.

Introduction

Vascular endothelial cells (VECs), which line all blood vessels and comprise the interface between blood and surrounding tissue, are a key to understanding pathologies and treatments of vascular systems, dictating numerous vascular functions critical to homeostasis and drug delivery thoughout the body[1,2]. Their governing functions[3] include permeability[4], angiogenesis[5], cell migration, proliferation, and apoptosis[6], impacting processes involved in inflammation[7], thrombosis[8], metastasis[9], and drug pharmacokinetics, all of which play critical roles in pathology and treatment of the two leading causes of death in the US[10]: cancer[11] and cardiovascular disease[12], as an example.

VECs have been found to delicately regulate such functions in response to dynamic microenvironments, and one major environmental parameter is the shear stress experienced at the vessel wall, or wall shear stress (WSS), induced by the flow of blood through the vasculature. VECs are reported to experience **mechontransductive effects on cell phenotype** when exposed to WSS via membrane-bound mechanosensors[13-15] (Fig. 1A). Such effects include the induced modulation of a myriad of biomolecular pathways leading to various physiological responses[16], such as resistance to apoptosis[19,20], upregulation of tight junction proteins (ZO-1, occludin)[17], extracellular matrix components (fibronectin, laminin)[18], membrane-bound efflux transporters (P-gp)[19] and integrins[20], as well as cytoskeletal restructuring and cell reorientation in relation to the flow direction[21-26]. The effects caused by WSS impact VEC functions relevant to pathology. For example, atherosclerosis, the leading cause of heart attack and stroke[27], has been correlated with low stress regions[28], while atheroprotective responses have been observed in high-stress regions[29], and WSS as high as 300 dyn/cm^2 has been measured in cases of vessel stenosis[30]. This variability in cell microenvironment indicates the need for comprehensive understanding of the adaptive responses of VECs to the WSS applied by the highly dynamic, highly variable microenvironment of the *in vivo* vasculature, and for delineating the practical limitations of dynamic *in vitro* culture conditions.

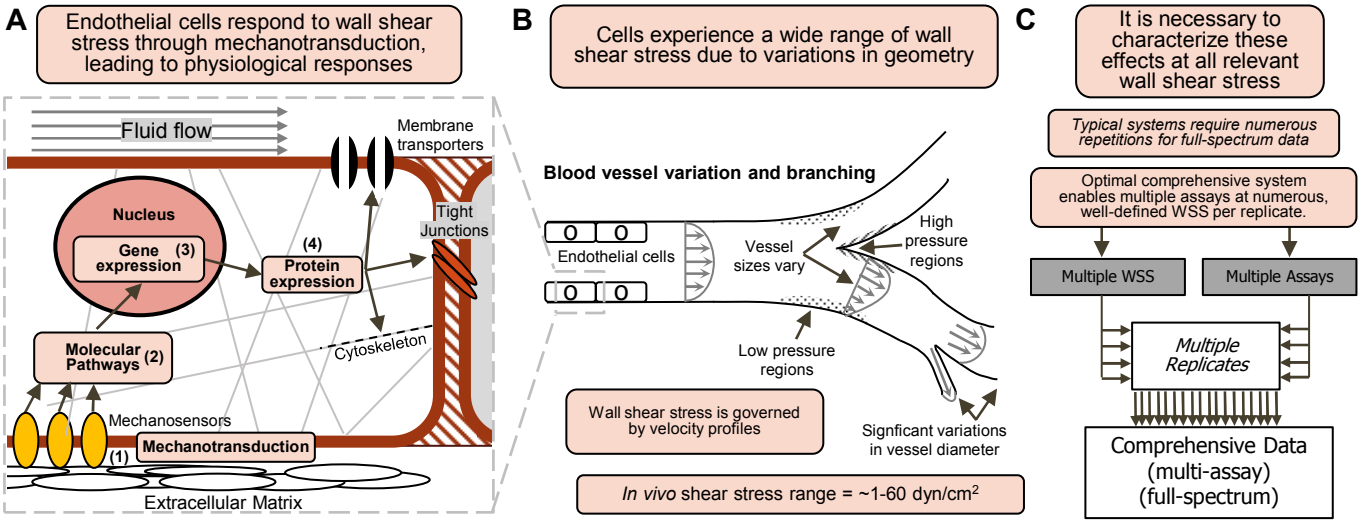

Fig. 1 Studying the relationship between vascular wall shear stress (WSS) and endothelial cell (EC) physiology. (A) VECs respond through mechano-transduction via mechanosensors (integrins and kinases), ultimately leading to significant changes in protein expression, such as in membrane transport, tight junctions, and cytoskeletal re-organization. (B) The WSS experienced by vascular endothelial cells varies significantly (1-60 dyn/cm^2) at different geometric locations *in vivo*. (C) An optimal, fully comprehensive approach to testing the relationship between WSS and VEC responses requires multiple well-defined, discrete WSS, and extraction of data via multiple assays, including trans-membrane testing, per replicate chip.

The study of VECs' responses to WSS has remained quite challenging both *in vivo* and *in vitro,* due to the difficulty in realizing the wide range of WSS conditions (**1-60dyn/cm^2**)[31] *in vivo*, and utilizing it for comprehensive assays. Such a large WSS range is mainly caused by significant variations of vessel sizes (8μm-2.5cm) and their differently localized pressure[32] (Fig. 1B). *In vivo* investigation does not provide reproducible and controllable testing conditions due to natural variations in tissue complexity and structural contiguity, forbidding precisely defined correlations between WSS and VEC response. *In vitro* methods, despite providing greater experimental control and repeatability of flow conditions[33], have failed thus far to effectively provide characterization spanning the physiologically relevant full spectrum of WSS. This is because all previous VEC cultures systems for assaying WSS effects (Tab. 1) are either limited to a single WSS condition per unit[13,21,24,25,34-43], or are limited in the types of feasible assays, due either to a lack of an integrated membrane[44] (preventing assays of barrier properties), or to non-uniformity in applied WSS among a cell population under assay[45-50] (preventing reliable correlation of assay results with discrete WSS). Though recently a closed-loop braille-display device has applied distinctly different WSS to three parallel channels[22], it covered only a limited shear stress range of <12dyn/cm^2 due to the limited flow rates from the integrated micro pumps and did not allow trans-monolayer assay. In summary, no VEC culture system has simultaneously achieved (1) multiple on-chip WSS conditions for isolated cell populations, while (2) allowing trans-membrane assays yet.

To address such issues, we have developed a **multi-channel and multi-assay platform** (Fig. 1C) where a single fluidic input produces multiple distinct WSS magnitudes homogenously applied to isolated VEC populations cultured on membranes, allowing multiple types of assays in a reproducible and controllable manner. To allow rapid characterization spanning the full *in vivo* WSS range (1-60dyn/cm^2), the platform employed four parallel channels producing distinct WSS with ~15x range of magnitude. In practice, by compounding the on-chip WSS variance with varying input flow-rates, useful quantitative data spanning the full spectrum of WSS can be efficiently gathered from a single experimental pump setup, and seeded from a single standard plate (75cm^2) of VECs (Fig. 2). For example, 8 chips in parallel in a standard 16-cartridge pump, compounded by varying input flow rates to each chip, will result in 32 distinct WSS. Furthermore, the designed ~15x magnitude range allows a single test to cover the full span of WSS experienced in brain capillaries (3-20dyn/cm^2)[51], which is the origin of the cell line used in this characterization study. Thus, the presented approach massively reduces required cells/reagents and turn-around time, while allowing unprecedented high-throughput, comprehensive WSS characterization assays. To allow trans-membrane assays, including trans-endothelial electrical resistance (TEER) and permeability, this platform employs the cross-junction structure used in our previously reported microfluidic BBB model[39].

Tab. 1 Comparison of flow-based *in* vitro systems for characterizing WSS effects on vascular endothelial cells.

Dynamic *in vitro* platforms for characterization of wall shear stress effects on vascular endothelial cells			
System type	**Multiple WSS conditions per unit**	**Isolated cell populations with homogenously applied WSS**	**Trans-monolayer assays**
Presented microfluidic system	***Yes***	***Yes***	***Yes***
Microfluidic (braille closed-loop)[22]	Yes	Yes	No
Rotational systems[45-47]	Yes	No	Yes
Microfluidic (geometric variation)[48-50]	Yes	No	No
Hollow fiber / capillary systems[19,47]	No	Yes	Yes
Microfluidic (constant-width channels)[24,34-39]	No	Yes	Yes
Parallel-plate flow chambers[13,21,25,40-43]	No	Yes	Yes

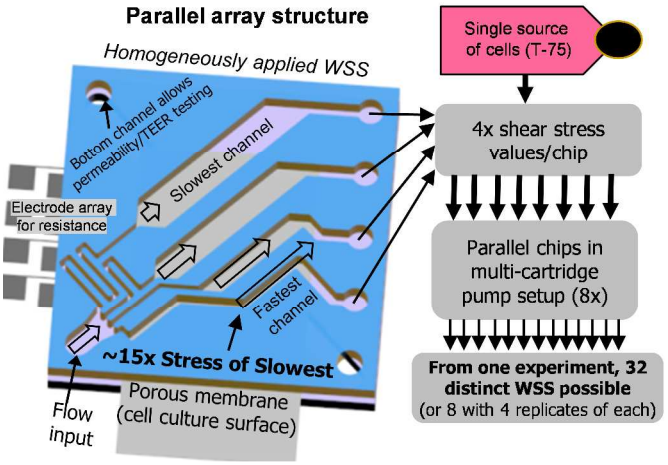

Fig. 2 The presented parallel channel array allows multiple high-throughput characterization assays of WSS effects on cultured endothelial cells. Four channels subject independent populations of endothelial cells to homogeneous WSS level at a ~15x range. Thus, from a single culture plate source with 8 chips in parallel in a single peristaltic pump setup, 32 quantitative shear stress assay datapoints can be achieved per experiment, spanning the full physiological WSS range (1-60dyn/cm^2) with replicates.

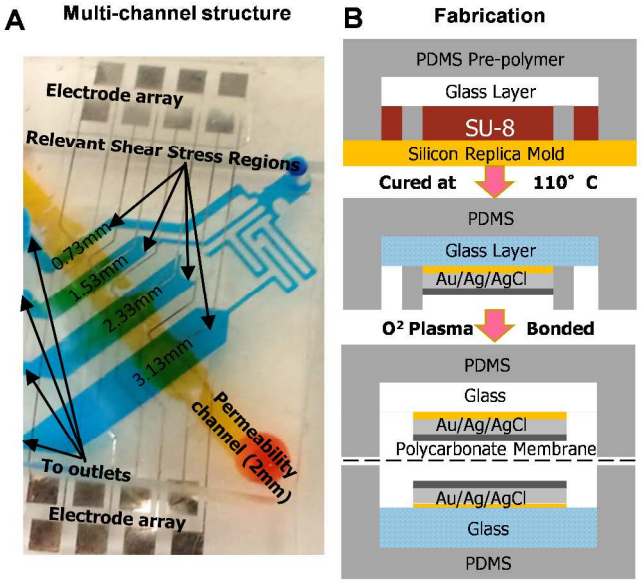

Fig. 3 (A) Multi-channel structure comprises 4 channels branched from a common inlet, exerting homogenous WSS at 4 distinct values to VECs cultured in the channel. A 2mm channel is fixed below, with a free-standing porous polycarbonate membrane as the culture surface. (B) To fabricate the multi-layered microfluidic devices, sputter-deposited glass electrode layers were embedded in PDMS pre-polymer (10:1) over a lithographically defined SU-8 mold and cured at 110°C. Channel layers and an APTES-treated polycarbonate membrane were bonded together with O^2 plasma activation.

This paper reports the design, fabrication, and testing results of the developed multi-channel, multi-assay WSS platform. To evaluate the effectiveness of the platform to produce a wide range of WSS, quantitative testing results are discussed, including velocity discretization into parallel channels (1) by COMSOL simulation and (2) by experimental measurements with an integrated micro-flow sensor array. Next, the validity of the platform as a high-throughput tool to correlate full-spectrum WSS effects with VEC properties of a particular cell line was quantitatively verified on the brain microvascular endothelial cell line bEnd.3 by measuring (3) cell morphology (cell elongation and orientation), (4) trans-monolayer permeability, (5) monolayer TEER, and (6) protein expression of tight junctions (ZO-1) and membrane-bound efflux transporters (P-gp).

Structures and Fabrication

To produce high-variance WSS distributions, a parallel array microfluidic structure of four channels was fabricated utilizing standard PDMS processing techniques to have significant differences in fluidic resistance among the channels, causing variations in the flow velocities and thus the resultant WSS.

Microfluidic Parallel-Channel Structures

The parallel array platform consists of four top (luminal) channels and one bottom (abluminal) channel that cross perpendicularly, all of which were constructed from multiple stacked poly-dimethylsiloxane (PDMS) layers (Fig. 3A). The four luminal channels branch from one common inlet and have independent outlets to simplify fluidic control and enable high-throughput parallel permeability assays. The four luminal channels have discrete widths (e.g. 0.73, 1.53, 2.33, 3.13 mm) with varying geometries at the branching region, subsequently causing different fluidic resistances, flow velocities and uniform WSS in each channel. When these channels were constructed in multiple layers by stacking PDMS substrates, a porous polycarbonate (PC) membrane was inserted to be free-standing at the channel junction, providing a monolayer cell culture surface allowing trans-monolayer assays (permeability/TEER) at each junction, as in the previously described μBBB system[39]. Flanking both sides of each PC culture surface, a set of thin-film AgCL electrodes were located to monitor TEER in the standard four-point sensing configuration minimizing error from parasitic resistance from external wires and contacts. The channel heights were initially set at 200μm, ensuring laminar flow and maximizing aspect ratio of the channels for WSS uniformity.

The platform structure was fabricated (Fig. 3B) similarly to the previously described μBBB system[39] with some modifications. First, embedded electrodes for TEER measurement were fabricated on a glass wafer by sputtering Cr/Au/Ag (20/80/800nm) and patterning layers using liftoff lithography (LOR-10B photoresist). The silver (Ag) surface was chlorinated with 30mM $FeCl_3$ for 50s to convert it into AgCl for corrosion resistant electrodes. Next, the channels were constructed among multiple PDMS layers. Channel molds were lithographically constructed from SU-8 2075 (200μm thick) on a silicon substrate, and silanized overnight with tridecafluoro-1,1,2,2-tetrahydrooctyl trichlorosilane in a vacuum chamber to minimize stiction and ease the separation during the molding process. On top of the SU-8 mold, PDMS layers were sequentially cast (10:1 elastomer:curing agent) and heat-cured (110ºC, 30m). Following 30 minutes pre-treatment of the PC membrane with 5% 3-aminopropyltriethoxysilane (APTES) at 80°C[52], a reliable bond between the membrane and PDMS channel layers was generated with O^2 plasma (125W, 20s) at 25°C. Residual APTES on the membrane was dissolved in ethanol. This bond method significantly decreased occurrences of leaks under high flow compared with the standard method using spin-coated PDMS pre-polymer[53], with no observed losses of cell adhesion. To generate the minimum total protein required for western blot (>25 μg), a large 5mm-wide, 175mm-long microfluidic channel was separately constructed.

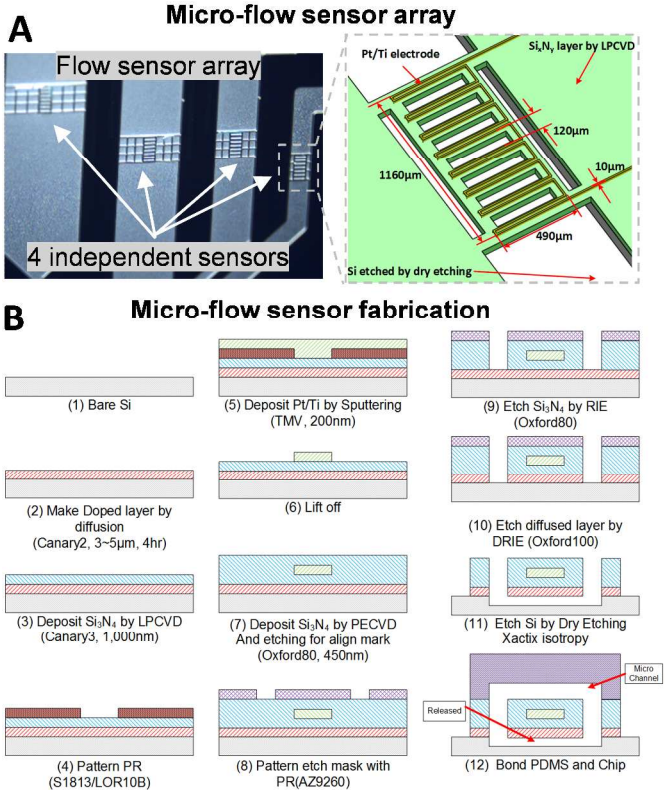

Fig. 4 (A) Fabricated micro-flow sensor array to measure WSS distributions in the parallel array structure. The mico-flow sensor structure is the same for all four channels, except the connecting bridge structure. (B) Fabrication process for the integrated micro-flow sensor in each microchannel. The sensor was fabricated on a N-doped silicon substrate by depositing LPCVD nitride, lift-off patterning 10μm wide Pt/Ti electrodes, depositing PECVD nitride, then layer and bulk etching the sensor structure with RIE, DRIE, and Xactix to generate the partially suspended structure.

Integrated Micro-Flow Sensor Array

In order to directly measure the WSS distributions in each micro channel and confirm the simulation results, a micro-flow sensor array was fabricated and integrated into the channel (Fig. 4A). The flow sensor utilized a standard suspended thermal conductivity detector (TCD) configuration[54]. An identical free-standing flow sensor was suspended in each channel at 70μm above the bottom wall. Each flow sensor consists of a meander-shaped 10μm wide electrode suspended over an area of 1160μm by 490μm above a channel. The interval between adjacent electrode crossings was 120μm, while the total length of the meander sensor was 7.8mm.

The micro-flow sensor was fabricated with standard microfabrication techniques (Fig. 4B). First, LPCVD (1μm) silicon nitride was deposited on a Si substrate, followed by sputter deposition of Pt/Ti layers (200nm/10nm), which was patterned to form 10μm wide sensor signal feed-through lines to the electrical pads. The Pt/Ti layer was then electrically passivated by another layer of patterned PECVD silicon nitride (450nm). Then the passivation layer was etched by RIE defining the sensor structure. Utilizing the same mask, anisotropic DRIE and isotropic Xactive XeF_2 etching were combined to etch the silicon substrate and partially suspend (with columns) the sensor structure at 70μm from the channel surface. Finally, the fabricated substrate was bonded to a 130μm PDMS channel structure, completing the structure of the final platform.

Cell Culture

The cell line tested in this study was the brain endothelial cell line bEnd.3[55]. The cells were grown with DMEM/F12 (Lonza), and was supplemented with 10% fetal bovine serum (Hyclone), 1% Penicillin/Streptomycin and amphotericin B (EMD). Media pH was buffered to ~7.35 for all experiments. All cells used for experiments were taken from confluent cultures only, within two days after confluence was reached. All cell cultivation and shear stress experiments were carried out in a humid incubator (Nu-Aire Autoflow 4750) with 5% CO_2 kept at a constant 37°C. Cell suspensions were centrifuged in an Eppendorf 5810, and all sterile work was performed in a class II biosafety cabinet (Thermo Fisher). Sterilization of microfluidic devices and tubing was carried out with 70% ethanol and UV radiation prior to use. A single T-75 flask was sufficient for seeding a parallel array of microfluidic cell culture models for shear stress experiments. Antibodies used in this study were: Primary rabbit anti-ZO-1 (GeneTex GTX108592), primary rabbit anti-MDR-1 (Santa Cruz sc-8313), primary rabbit β-actin (Abcam ab8227), secondary HRP-conjugated goat anti-rabbit (Abcam ab6721), and secondary Alexa Fluor 488 goat anti-rabbit (Molecular Probes A-11008).

Testing methodology

First, the fabricated platform was evaluated on its capability of producing a wide range of WSS by (1) predictions based on analytical calculation and simulations and (2) direct flow velocity measurement from the integrated micro flow sensor array. Next, the validity of the platform as the high-throughput tool to correlate full-spectrum WSS effects with VEC properties was evaluated by monitoring the (3) cell morphology (shape and orientation angle), (4) trans-monolayer permeability, (5) TEER, and (6) protein expression of tight junctions and efflux transporters of the bEnd.3 cell line.

Prediction of the Wall Shear Stress by Simulation

In order to predict the resultant WSS levels that cells experience at the channel wall, (1) fine-mesh 3D COMSOL simulations were performed to obtain velocity profiles at different heights from the wall; (2) shear rate *dU/dz* at the wall was calculated by COMSOL based on the velocity gradient right above the wall; (3) shear rate was multiplied with the proportionality constant μ, or viscosity, as in the following equation (Fig. 5A) [56]:

$$\tau = \frac{dU}{dz}\mu \qquad (1)$$

COMSOL simulation utilized the laminar flow module that derives velocity fields from the Navier-Stokes Equations. Assumptions used in the model were Newtonian fluid (μ=1.2mPa·s for media with serum), the no-slip condition, with equal pressure at all outlets. Note that the COMSOL simulations and analytical calculations also assumed that all flow in each of the described devices at all relevant flow-rates is completely laminar, with a Reynolds number several orders of magnitude lower than the turbulent threshold (2300), which is a reasonable assumption in microfluidics[57]. It was assumed that the effects of flow-induced deformation of the channel walls[58] was negligible at all relevant flow-rates for the study, and that the channel walls remained rigid for the purpose of WSS calculation and measurement in this study.

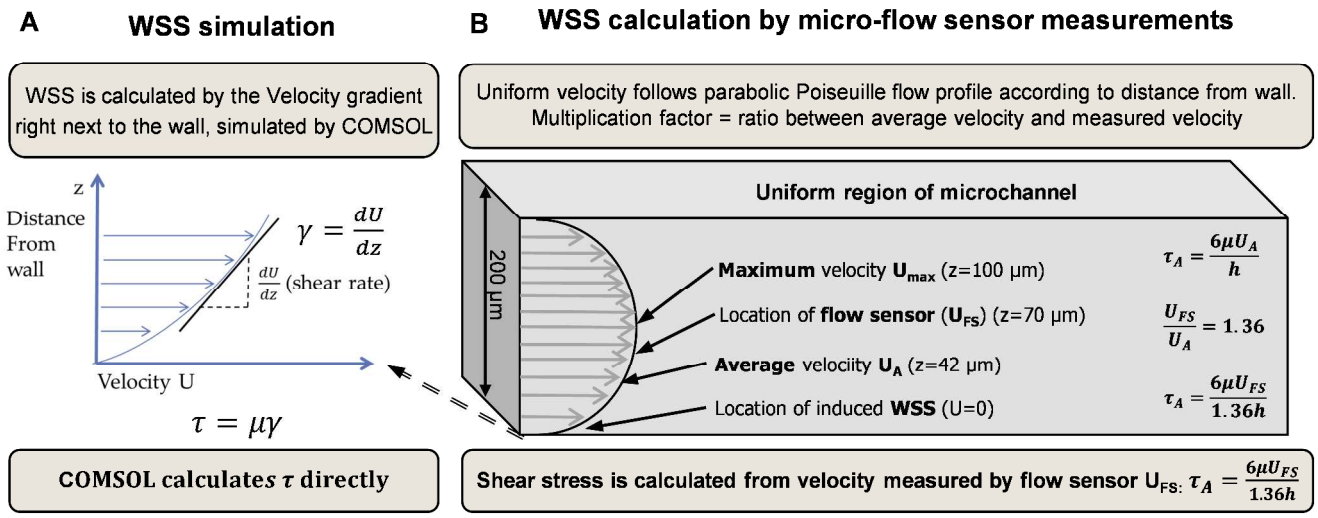

Fig. 5 Shear stress calculation methods. All channels are 200 μm high. (A) WSS was simulated by COMSOL based on the vertical velocity gradient *dU/dz* multiplied by the dynamic viscosity μ. (B) Uniform velocity (70 μm height) measured by the micro-flow sensor was used to calculate the average shear stress τ_A based on the standard equation for shear stress in a rectangular micro-channel based on the average velocity U_A. The ratio between U_A and U_{FS} is 1.36, so this multiplication factor was used to derive the average wall shear stress equation for micro-flow sensor measurements.

Shear Stress Measurement with Integrated Micro Flow Sensors

In parallel to COMSOL simulation, the average WSS (τ_A) at the wall was calculated from the velocity measurement by the fabricated micro flow sensor (U_{FS}) in each channel (Fig. 5B). Since the fabricated micro sensor was located at 70μm above the wall, the measurement does not directly represent the average velocity (located at 42μm height for our device), necessitating an adjustment process in order to utilize the well-established relationship between the average velocity (U_A) and τ_A in a rectangular channel[56]. For this adjustment, the ratio between U_{FS} and U_A, as obtained from the Poiseuille flow velocity profile in the vertical direction of the channel, was found to be ~1.36, and was applied as a multiplication constant to the denominator of the standard equation for average WSS in a rectangular channel[56], allowing calculation of τ_A from U_{FS}:

$$\tau_A = \frac{6\mu U_{FS}}{1.36h} \quad (2)$$

where h is channel height and μ is the dynamic viscosity.

To prepare for the induction of WSS into the parallel channels, fluidic interconnection was established by sealing marprene or silicone tubing (0.25, 0.38, 0.76, 1.0, 1.59mm) to the inlet ports (DC734 adhesive) with 22 or 18 gauge needles and 200μl pipet tips. Through the ports, fluid was manipulated with a 16-cartridge peristaltic pump (Watson-Marlow 205S). Then, measurement utilizing the fabricated micro flow sensor was performed, while certain flow rates were supplied through the platform. The terminals of the micro flow sensors were connected to a Wheatstone Bridge circuit to measure voltage offsets resulting from differential thermal dissipation. Defined flows of DI water from a steady-flow syringe pump (KDS210) were injected in reverse through the outlets to generate calibration curves for each sensor. Electrical measurements were made with a power supply (GW Instek PSP603) and an NI DAQ. After 10s continuous flow, thus when flow is stable, 5V was applied and output voltage was recorded (10s, 1kHz) through the DAQ. Following brief cooldown, the process was repeated at least three times. To measure the velocity distributions under forward flow, known flow rates were injected through the inlet, and the measured voltage outputs in each channel were fitted to their calibration curves to calculate uniform velocity.

For further comparison, volumetric flow measurements (at least 3 replicates) at the outlet of each chip were fit to the standard equation for average WSS:

$$\tau_A = \frac{6Q\mu}{h^2 w} \quad (3)$$

Application of Shear Stress to Cultured Endothelial Cells

To analyse physiological effects of WSS on confluent cultures, the platforms were prepared by sealing marprene or silicone tubing to inlet ports in connection to a 16-cartridge peristaltic pump. Permeability/TEER measurement required two dedicated cartridges, and imaging & western blot measurement required one dedicated cartridge. Depending on tubing volume, 8-well strips (300 μL) with poly-tetrafluoroethylene plugs or centrifuge tubes lined with parafilm were used as media reservoirs. The entire experimental setup (pump, platforms, and reservoirs) was placed in a CO_2 incubator. Though flow-rates differed among the four parallel channels, they were appropriate for simultaneous cell seeding and channel flushing to be practical. To culture cells in the fabricated platform, the platform was sterilized first with 70% ethanol and coated overnight with fibronectin and collagen IV (100μg/mL each) to facilitate cell adhesion. After sterilization b.End3 cells were seeded in the devices at a density of $6e^4/cm^2$ and allowed to adhere in a static condition (no flows) for 2h. Then the platforms were flushed with sterile DMEM/F12 media and perfused at very low flows (uncharacterized minimum pump setting) for 3 days to allow cell confluence and optimal cell anchorage. Media reservoirs were changed daily. Experimental WSS was applied for 24h prior to quantitative assays to characterize the WSS effects on bEnd.3 physiology.

Morphometric analysis

In order to evaluate the shear stress effects on cell morphology, VECs were imaged on-chip and both shape and orientation angle of the cells were analyzed with CellProfiler software, while various WSS was applied to each channel. For cell

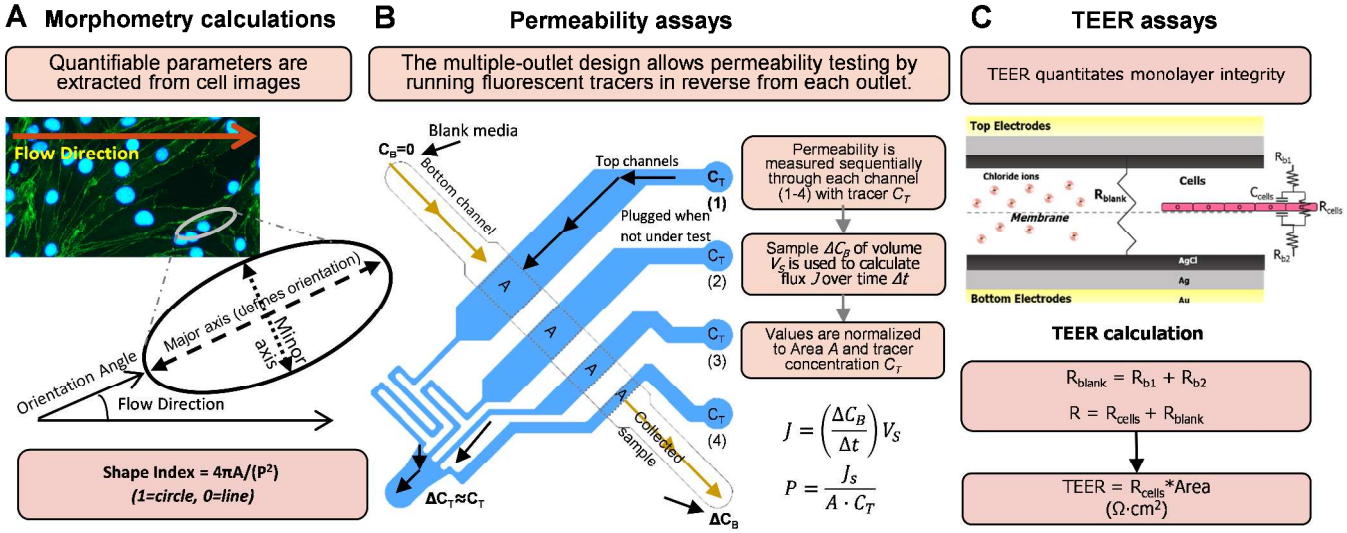

Fig. 6 Testing methodology. (A) Morphometry calculations. To quantify ZO-1-tagged images taken at different WSS, dimensions and orientations were analyzed with CellProfiler software, providing orientation angle away from flow direction, and shape index, defining properties of each cell. (B) Permeability assays. Fluorescent tracers of concentration C_T were sequentially flowed in reverse through each channel outlet (with the other three outlets plugged) and flux was calculated by measuring tracer concentration in the bottom channel perfusate, and was normalized to channel junction area and top concentration to give permeability coefficients. (C) TEER assays. To measure monolayer integrity, TEER was measured by connecting electrode terminals to an EVOM epithelial voltohmeter, and cell resistance was found by subtracting readings by blank membrane measurements, and transformed by area to give TEER values.

imaging preparation, monolayers of b.End3 cells were fixed with 4% paraformaldehyde (Avantor) for 20 min at room temperature. Cell membranes were permeabilized with 0.1% Triton X-100 in PBS for 20 minutes. Cells were then blocked for 1 hour under gentle rotation with 5% bovine serum albumin in permeabilization buffer, and cells were incubated overnight at 4°C with anti-ZO-1 primary antibody. Cells were then incubated with Alexa-fluor 488-conjugated secondary antibody for 1 hour under gentle rotation. To visualize the cells, they were imaged with a fluorescent Nikon microscope. To quantitatively assess changes in cell morphology under various WSS, images were processed with CellProfiler to measure cell dimensions and positions (Fig. 6A), modeling cells as ellipses.

To quantify cell elongation, we used shape index *(SI)*

$$SI = \frac{4\pi A}{P^2} \quad (4)$$

where A=area and P=perimeter. An object with SI of 1 is a circle, and SI of 0 is a straight line. To quantify cell alignment, the orientation angle (OA) is defined as the angle (0-90°) between the cell's major axis and direction of flow. Negative orientation angles were inverted to their positive values.

Permeability assay

In order to evaluate the shear stress effects on the cross-membrane transfer of molecules, the permeability of two commonly used fluorescent tracers, fluorescein isothiocyanate (FITC)-dextran (4kD size) and propidium iodide, was monitored in each channel in reference to the corresponding WSS values. Fluorescent tracer concentrations were measured with a BioRad Synergy plate reader for FITC-Dextran 4k (490/525nm excitation/emission) and propidium iodide (536/617nm), and fitted to known standards to calculate the concentration values. Then, the concentration values were utilized to calculate the corresponding permeability (Fig. 6B).

The tracer flux J through the cell layer was measured with the following flux equation

$$J = \left(\frac{\Delta C_B}{\Delta t}\right) V_S \quad (5)$$

where ΔC_B is bottom perfusate concentration change, Δt is assay time, and V_S is bottom perfusate sample volume. Permeability coefficients were calculated[59,60] for each tracer with the conventional equation for permeability

$$P = \frac{J_S}{A \cdot C_T} \quad (6)$$

where P is the permeability coefficient, A is culture area, and C_T is the concentration being flowed through the top channel. To normalize values for blank membrane flux, endothelial coefficients P_e were calculated by subtracting the inverse of the measured P value by the inverse of coefficient P_b through a blank membrane (no cells), as in the following equation[61].

$$\frac{1}{P_e} = \frac{1}{P} - \frac{1}{P_b} \quad (7)$$

TEER assay

TEER values were measured under various WSS levels to evaluate the changes in confluence and integrity of tight junctions. For measurement of TEER (Fig. 6C), voltage and current electrode pads were connected through 30-gauge wires with conductive silver epoxy via an electrode adaptor (WPI) to an EVOM2 epithelial voltohmeter (WPI). The EVOM2 passes a constant 10μA AC current at 12.5Hz while measuring resistance changes. To calculate TEER, initial D0 Background resistances R_{blank} were subtracted from measured resistance following 24h WSS R, and normalized for the cell culture area for that particular channel, giving TEER values in Ωcm^2 from the following equation.

$$TEER = (R - R_{blank})A \quad (8)$$

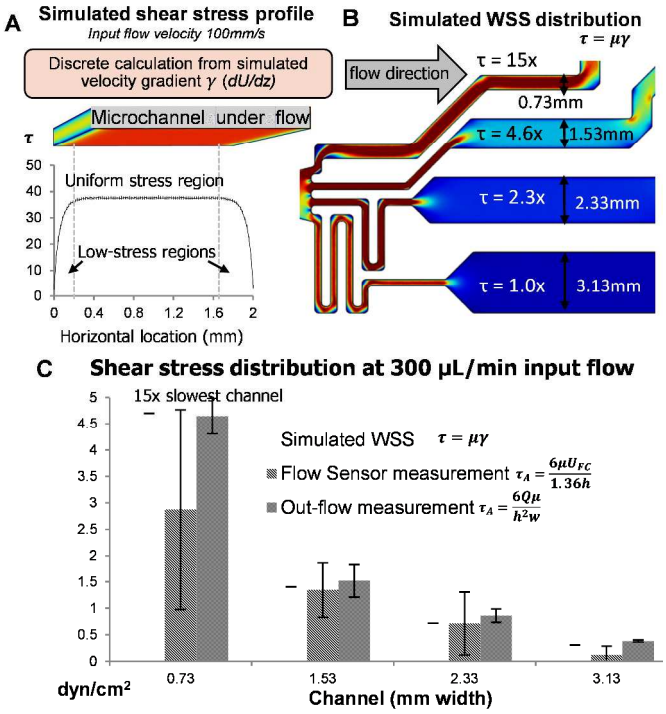

Fig. 7 WSS characterization results. (A) Horizontal WSS profile in the channel is largely uniform, between the high-drag regions (~200 µm) by either sidewall of the channel. (B) WSS distributions were found by COMSOL simulation to be 15, 4.6, and 2.3 times the minimum value for the parallel array, based on the vertical velocity gradient *dU/dz* adjacent to the wall in each channel. (C) Shear stress distributions between the four channels at 300 µL/min were compared between simulation results, micro-flow sensor measurements, and volumetric measurements of channel out-flows following timed perfusion. Values for the middle two channels were sufficiently equivalent, but there were discrepancies with the fastest and slowest channels for the flow-sensor results. Standard deviation error bars displayed, all test replicates were $n \geq 3$.

Western blot

Protein expression assays were performed to affirm the causes of physiological responses under various shear stress levels. Particularly, two proteins were monitored, tight junction component ZO-1 and membrane efflux transporter p-glycoprotein (P-gp), at multiple WSS because these proteins correlate with monolayer tightness and membrane transport activity. Cells were scraped from the channel substrate surface, or 6-well static controls, with a cell scraper and lysed. Following 10s sonication, total protein was centrifuged (12000RPM, 15m) and separated from pellet. Protein was quantified with BCA total protein assay, and 25µg protein was loaded in 4-12% Bis-Tris gels (Novex) and run at 200V for ~1h, or until sufficiently separated. Following 1h transfer to nitrocellulose membrane at 30V, membranes were blocked with 5% skim milk (1h) in TBS-Tween-20. Rabbit primary antibodies for ZO-1, MDR-1 (P-gp), and β-actin as a loading control, were incubated overnight at 4°C. Goat anti-rabbit horseradish peroxidase secondary antibody was incubated for 1h, and chemiGlow (AlphaInnotech) was applied to the membrane, and imaged for band analysis with a FluorChem FC2 imaging system.

Results and discussion

Shear Stress Simulation and Measurement

COMSOL simulation results indicated that the horizontal profile of velocity and WSS within a channel is largely uniform except the high-drag regions near the side-walls within a distance of ~200 µm (Fig. 7A). This uniformity helps optimize the homogeneity of the discrete WSS experienced by the cells in the channel, as it is desired to achieve as uniform an environment for all cells in a particular population. Due to the high-drag region, which is independent of channel width and only related to channel height, the proportion of cells experiencing lower shear stress is smaller for the wider channels, so the wider channels have a more homogenous profile, indicating the need for a high aspect ratio to optimize accuracy of WSS measurements. Though the high-drag regions in the smallest channel make up a slightly larger surface area than the uniform region (~330), its lower aspect ratio was necessary to achieve high WSS variance between channels.

COMSOL simulation results also showed that uniform WSS distribution among four channels were repeatedly achieved with the span ratio of ~15x relative magnitude between the fastest and slowest channels regardless of input flow-rate (Fig. 7B). Thus, the simulation results indicated that the full *in vivo* shear stress spectrum of 1-60dyn/cm^2 is achievable in as few as two parallel chips with two different input flow-rates of at least ~4x difference, allowing very rapid application and testing of the full physiological spectrum.

Figure 7C shows the COMSOL simulation results (eq. 1) in comparison to the micro-flow sensor measurements (eq. 2) and estimation from the volumetric measurements (eq. 3) at an example input flow-rate of 300 µL/min. The comparison revealed that all three values matched within 10% error for the two center channels, indicating the validity of both prediction and measurement methods. The WSS values from the micro flow sensors showed that the discrepancy becomes larger for the smallest (0.73mm) and largest (3.13mm) channel sizes by 22% and 66% of the simulated values, respectively.

Morphometric Analysis

Image analysis data from optical measurements showed that the bEnd.3 cells did not exhibit any notable change in shape index, a measure of cell elongation, with increases in WSS (Fig.8A). It is known that the tested cell line in this study (bEnd.3) holds a characteristic highly-elongated morphology under static conditions[55], and we hypothesize that this trait makes the cell line less susceptible to changes in *SI* than other cell types with a rounder, more "cobble-stone" morphology under static conditions. For example, human aortic endothelial cells with a static *SI* of 0.7 have exhibited a decrease to 0.4 at 12 dyn/cm^2 WSS[62], and bovine aortic endothelial cells with a static *SI* of 0.76 have also shown a decrease to 0.31 at 20 dyn/cm^2 WSS[63], while the utilized bEnd.3 cell line has initially low *SI* of 0.13 or 0.1 (mean) or 0.1 (median) at static condition.

Optical measurement data also showed that the cell lines adjusted their orientation with the flow direction under increasing WSS (Fig. 8B). The mean orientation angles respectively decreased from 45.3° to 18.1° under the WSS range from 0 (static) to the highest tested at 86 dyn/cm^2, while the overall trend of the mean values formed a linear correlation (R^2 of 0.61), suggesting an increase in cell alignment with increasing WSS. Residual analysis of the linear regression of the orientation angle data (R^2 of 0.05) indicated a right

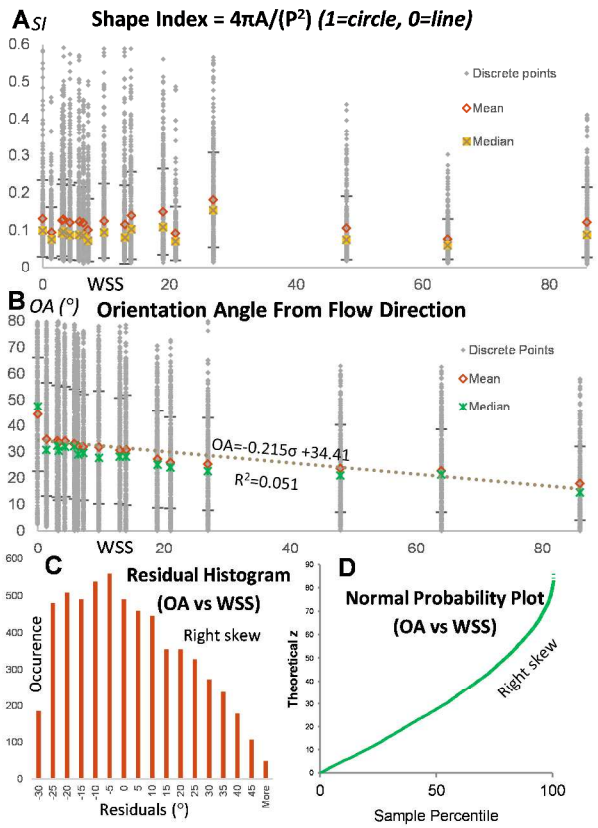

Fig. 8 Morphometry results. Each data-point represents measurements from an individual cell. Also displayed are mean and median values. (A) bEnd.3 cell shape index measurements with increased WSS. No trend was evident. (B) Linear regression analysis of orientation angle data suggested increased alignment, with an R^2 of 0.051. Orientation angle showed a slight alignment along with WSS. The higher mean values than median values are expected, given the right (positive) skew indicated by the (C) residual histogram and (D) normal probability plot for the orientation angle regression analysis.

(positive) skew as indicated by the distribution of the residuals (Fig. 8C) and the normal probability plot (Fig. 8D). In congruence, the median values were consistently higher than the mean values, resulting in discrete mean and median values in Fig. 8. Median values also showed a linear decrease along with WSS, ranging from 47.6 to 14.6 for static control and 86 dyn/cm^2, respectively.

Permeability

Experimental measurement results demonstrated that the permeability of chemical compounds decreased with increasing WSS. Fig. 9 shows the resultant permeability coefficients of fluorescent tracers FITC-Dextran 4kD (Fig. 9A) and propidium iodide (Fig. 9B). The permeabilities of FITC-dextran and propidium iodide decreased from averages of 7.4e^{-6}cm/s and 2.3e^{-5}cm/s to 4.0e^{-6}cm/s and 1.9e^{-5}cm/s, respectively with increasing WSS from 0.35 to 86 dyn/cm^2. The decreasing rates for the permeability of the fluorescent tracers were 4.06e^{-8}cm/s and 6.04e^{-8}cm/s per dyn/cm^2 for FITC-Dextran and PI, respectively. Minimum and maximum average values ranged from 7.4e^{-6}cm/s and 2.3e^{-5}cm/s (0.35dyn/cm^2) to 4.0e^{-6}cm/s and 1.9e^{-5}cm/s (86dyn/cm^2) for FITC-Dextran 4kD and PI, respectively. A reduction in standard deviation was observed at WSS above 20 dyn/cm^2. Though FITC-Dextran's mean value increased slightly from 64 to 86 dyn/cm^2, the mean values fall

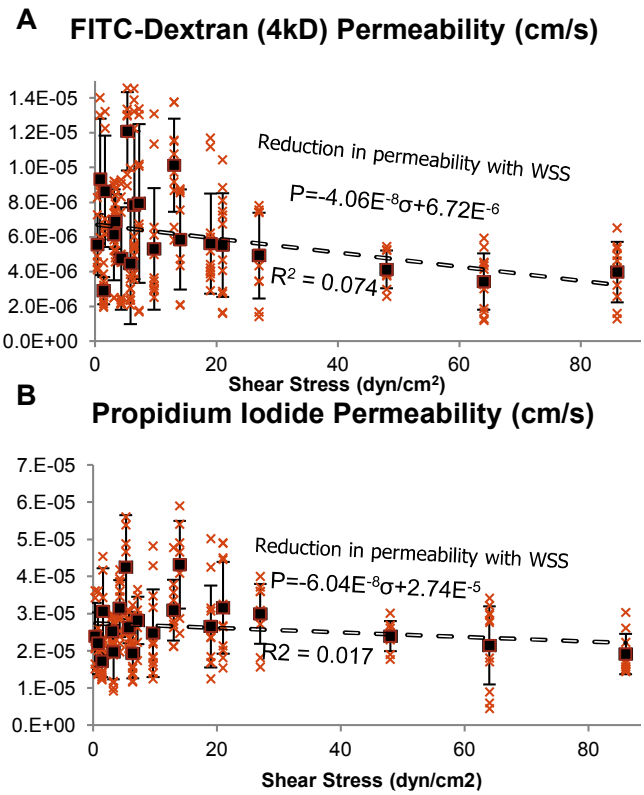

Fig. 9 Permeability of FITC-conjugated Dextran 4kD (A) and propidium iodide (B) at WSS magnitudes ranging from 0.35-84dyn/cm^2 indicated a decrease in permeability with increasing WSS, at -4.06e-8 and -6.04e-8 unit permeability/unit WSS, respectively. Standard deviation was notably reduced at WSS higher than ~20 dyn/cm^2. All sample replicates n>8.

within a standard error of each other. For all conditions, the tests were repeated at least 8 times (n>8).

Permeability was consistently higher for propidium iodide than for FITC-Dextran. This agrees to the expectation based on the lower molecular weight (668D) than FITC-Dextran (~4kD), making diffusion more rapid. Note that for FITC-Dextran at higher WSS (near 86dyn/cm^2) the increased mean permeability may indicate a slight loss of cell adhesion, but the increase is not significant, and was not observed in the propidium iodide permeability data, nor was a decrease in TEER observed. Potential issues with cell adhesion are cell line-specific, so testing of other cell types with reduced anchorage strength may potentially indicate losses in anchorage with the presence of "pinholes", or missing cells in the monolayer, increasing permeability at higher WSS. The bEnd.3 cell line was selected for the testing due to their characteristic high surface adherence.

TEER

TEER was measured with the independent electrode sets to evaluate monolayer integrity under varying flow conditions. In correlation with the permeability results in Fig. 10, the measurement data showed that there was an increase in TEER (Fig. 10) with increasing WSS at a rate of 0.8Ωcm^2 per dyn/cm^2, ranging from 183Ωcm^2 at near-static 1.4dyn/cm^2 to 230Ωcm^2 at 86dyn/cm^2. As with the previously discussed permeability results, apparent anchorage losses resulting in reduced TEER was not observed at high WSS.

It is noteworthy to mention that a consensus exists for BBB models that TEER levels must exceed 150Ωcm^2 for reasonably

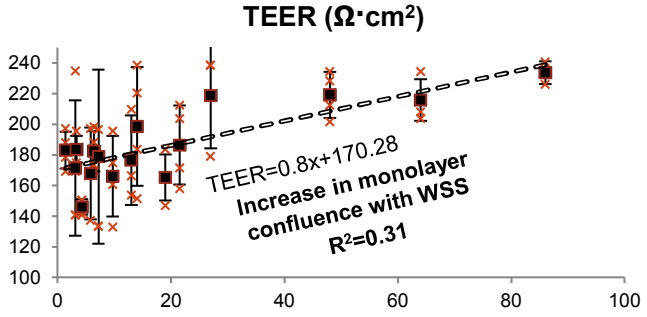

Fig. 10 TEER measured following high shear stress was increased at about 0.8 unit resistance/unit WSS. These data indicate increased barrier tightness with higher WSS, in correlation with permeability results. All replicate n>3.

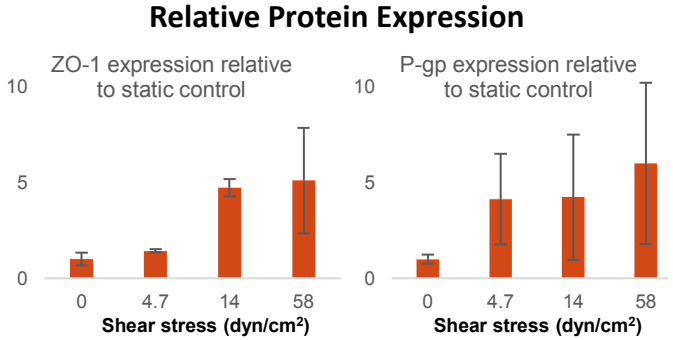

Fig. 11 Densitometric relative band analysis for western blots from cell lysates of brain endothelial cells grown to confluence and exposed to 24h WSS were compared with static controls grown in 6-wells. Results are weighted to β-actin as a gel loading control. Static control was derived from 6-wells plates. These data indicate significant increases in tight junction and efflux transporter expression under WSS at up to an average of ~5x and ~6x for ZO-1 and P-gp, respectively, at 58 dyn/cm^2 WSS. All replicate n>3.

representative permeability data to be obtained[64] in comparison to typical *in vivo* TEER levels (>1000Ωcm^2). The measured TEER values in this paper exceeded 150Ωcm^2 at all tested values of WSS. This also supports the use of the bEnd.3 cell line under the described culture conditions for use in BBB testing studies at high WSS of 60 dyn/cm^2, at the high end of the shear stress seen *in vivo*.

Western blot analysis

The protein expression analysis data provided by western blot analysis (Fig. 11), showed significant increases in expression of both tight junction component ZO-1 and efflux transporter P-gp under three distinct WSS, relative to static control derived from 6-well plates. The protein expression relatively increased ~5x for ZO-1 and ~6x for P-gp at 58 dyn/cm^2 compared to the static condition (0 dyn/cm^2). Notably, a larger relative increase in ZO-1 was observed at 14 dyn/cm^2 (~5x), while P-gp expression increased significantly (~4x) at 4.7dyn/cm^2.

Both proteins are known to influence trans-monolayer properties, such as permeability and TEER; thus the increase in the measured value in protein expression under increasing WSS matches well to the results obtained in aforementioned methods: reduction in permeability and increase in TEER with increases in WSS conditions.

Conclusions

This paper reported the design, fabrication, and testing results of the microfluidic platform that enables application of the WSS range (1-60dyn/cm^2) of the full physiologically relevant spectrum on vascular endothelial cells (VECs), while allowing multiple physiological, biochemical, and trans-membrane assays in a high throughput manner on a chip. To allow rapid full-spectrum characterization of WSS effects, we developed the four channel microfluidic platform that simultaneously produces shear stresses spanning ~15x in magnitude. Flow distributions were predicted with COMSOL simulation and verified by the direct measurement with a micro flow sensor array and volume measurement. Multiple assays were performed, including cell morphometry, protein expression, permeability and TEER, on the brain microvascular endothelial cell line bEnd.3.

Morphometric image analysis showed increased alignment with flow direction with increases in WSS. Permeability measurement exhibited decreasing permeability with increasing WSS at rates of 4.06e^{-8} and 6.04e^{-8}cm/s per dyn/cm^2 for FITC-conjugated Dextran and propidium iodide, respectively. TEER measurement data showed an increase with increasing WSS by a rate of 0.8 Ωcm^2 per dyn/cm^2. Finally, the Western blot results demonstrated notable increase in expression of a tight junction component ZO-1 and an efflux transporter P-gp by ~500% and 600%, respectively, compared to static controls. These results indicate that the bEnd.3 cell line responds to WSS *in vitro* in a magnitude-dependent manner, providing insights for optimal flow conditions for dynamic VEC culture models.

Based on the results, we also conclude that the presented microfluidic approach is a valid protocol for rapidly assaying physiological responses to the full spectrum of WSS, as well as elucidating limitations of practical flow conditions, for a particular combination of VEC cell line or primary cell type and culture conditions.

Acknowledgements

This research was supported by the Utah Science Technology and Research Initiative (USTAR). Microfabrication was performed at the University of Utah Nano Fabrication Facility located in the Sorenson Molecular Biotechnology Building. Western blot and microscopy was performed at the Furgeson Research Group in the Pharmaceutics Department at the University of Utah, with special thanks to Ms. Pilju Youn and Prof. Darin Furgeson.

Notes and references

[a] Department of Bioengineering, University of Utah, SMBB-3100, 36 S Wasatch Dr, Salt Lake City, UT, USA 84112. Tel: +1 208 861 5597; E-mail: Ross.Booth@utah.edu
[b] Department of Electrical & Computer Engineering, University of Utah, MEB-3280, 50 S Central Campus Dr, Salt Lake City, UT, USA 84112. E-mail: nohmoses@gmail.com
[c] Department of Electrical & Computer Engineering, University of Utah, MEB-3280, 50 S Central Campus Dr, Salt Lake City, UT, USA 84112. Tel: +1 801 587 9497; E-mail: Hanseup@ece.utah.edu

1 G. Bazzoni and E. Dejana, *Physiological Reviews,* 2004, **84**(3), 869.

2 P. Rajendran, T. Rengarajan, J. Thangavel, Y. Nishigaki, D. Sakthisekaran, G. Sethi, and I. Nishigaki, *International Journal of Biological Sciences,* 2013, **9**(10), 1057.
3 C. Michiels, *Journal of cellular physiology,* 2003, **196**(3), 430.
4 L. L. Rubin and J. M. Staddon, *Annu Rev Neurosci,* 1999, **22**(11.
5 M. E. C.-s. Angiogenesis and P. Factor, *The Journal of cell biology,* 1995, **129**(4), 895.
6 S. Chien, *Am J Physiol Heart Circ Physiol,* 2007, **292**(3), H1209.
7 A. Mantovani, F. Bussolino, and E. Dejana, *The FASEB journal,* 1992, **6**(8), 2591.
8 J. D. Pearson, *Best Practice & Research Clinical Haematology,* 1999, **12**(3), 329.
9 G. J. Gasic, *Cancer and Metastasis Reviews,* 1984, **3**(2), 99.
10 A. M. Miniño and S. L. Murphy, *NCHS data brief,* 2012, **99**(10), 1.
11 M. A. Moss, S. Zimmer, and K. W. Anderson, *Anticancer research,* 2000, **20**(3A), 1425.
12 A. A. Quyyumi, *The American journal of medicine,* 1998, **105**(1), 32S.
13 E. Tzima, M. Irani-Tehrani, W. B. Kiosses, E. Dejana, D. A. Schultz, B. Engelhardt, G. Cao, H. DeLisser, and M. A. Schwartz, *Nature,* 2005, **437**(7057), 426.
14 S. Chien, S. Li, and Y. J. Shyy, *Hypertension,* 1998, **31**(1 Pt 2), 162.
15 S. Chien, *Biorheology,* 2006, **43**(2), 95.
16 A. D. Acevedo, S. S. Bowser, M. E. Gerritsen, and R. Bizios, *J Cell Physiol,* 1993, **157**(3), 603.
17 V. Siddharthan, Y. V. Kim, S. Liu, and K. S. Kim, *Brain Res,* 2007, **1147**(39.
18 O. Thoumine, R. M. Nerem, and F. R. Girard, *In Vitro Cellular & Developmental Biology-Animal,* 1995, **31**(1), 45.
19 L. Cucullo, M. Hossain, V. Puvenna, N. Marchi, and D. Janigro, *BMC Neurosci,* 2011, **12**(40.
20 C. Urbich, D. H. Walter, A. M. Zeiher, and S. Dimmeler, *Circ Res,* 2000, **87**(8), 683.
21 C. G. Galbraith, R. Skalak, and S. Chien, *Cell Motil Cytoskeleton,* 1998, **40**(4), 317.
22 J. W. Song, W. Gu, N. Futai, K. A. Warner, J. E. Nor, and S. Takayama, *Anal Chem,* 2005, **77**(13), 3993.
23 H. Nakadate, H. Minamitani, and S. Aomura, *Conf Proc IEEE Eng Med Biol Soc,* 2010, **2010**(3812.
24 A. D. van der Meer, A. A. Poot, J. Feijen, and I. Vermes, *Biomicrofluidics,* 2010, **4**(1), 11103.
25 L. G. Braddon, D. Karoyli, D. G. Harrison, and R. M. Nerem, *Tissue Eng,* 2002, **8**(4), 695.
26 S. Chien, *Ann Biomed Eng,* 2008, **36**(4), 554.
27 P. Poredoš, *Clinical and Applied Thrombosis/Hemostasis,* 2001, **7**(4), 276.
28 A. M. Malek, S. L. Alper, and S. Izumo, *JAMA: the journal of the American Medical Association,* 1999, **282**(21), 2035.
29 R. S. Reneman, T. Arts, and A. P. G. Hoeks, *Journal of Vascular Research,* 2006, **43**(3), 251.
30 J. Dolan, J. Kolega, and H. Meng, *Annals of Biomedical Engineering,* 2013, **41**(7), 1411.
31 J. Loscalzo and A. I. Schafer, *Thrombosis and hemorrhage*. 2003: Lippincott Williams & Wilkins.
32 A. G. Koutsiaris, S. V. Tachmitzi, N. Batis, M. G. Kotoula, C. H. Karabatsas, E. Tsironi, and D. Z. Chatzoulis, *Biorheology,* 2007, **44**(5-6), 375.
33 E. W. Young and C. A. Simmons, *Lab Chip,* 2010, **10**(2), 143.
34 H. Chen, J. Cornwell, H. Zhang, T. A. Lim, R. Resurreccion, T. Port, G. Rosengarten, and R. Nordon, *Lab Chip,* 2013,
35 E. W. Young, A. R. Wheeler, and C. A. Simmons, *Lab Chip,* 2007, **7**(12), 1759.
36 S. Hsu, R. Thakar, D. Liepmann, and S. Li, *Biochem Biophys Res Commun,* 2005, **337**(1), 401.
37 J. Shao, L. Wu, J. Wu, Y. Zheng, H. Zhao, Q. Jin, and J. Zhao, *Lab Chip,* 2009, **9**(21), 3118.
38 R. Estrada, G. A. Giridharan, M. D. Nguyen, T. J. Roussel, M. Shakeri, V. Parichehreh, S. D. Prabhu, and P. Sethu, *Anal Chem,* 2011, **83**(8), 3170.
39 R. Booth and H. Kim, *Lab on a Chip,* 2012, **12**(10), 1784.
40 J. H. Dangaria and P. J. Butler, *Am J Physiol Cell Physiol,* 2007, **293**(5), C1568.
41 P. Fernandez, C. Bourget, R. Bareille, R. Daculsi, and L. Bordenave, *Tissue Eng,* 2007, **13**(7), 1607.
42 O. Thoumine, R. M. Nerem, and P. R. Girard, *In Vitro Cell Dev Biol Anim,* 1995, **31**(1), 45.
43 H. Miao, Y. L. Hu, Y. T. Shiu, S. Yuan, Y. Zhao, R. Kaunas, Y. Wang, G. Jin, S. Usami, and S. Chien, *J Vasc Res,* 2005, **42**(1), 77.
44 B.-h. Chueh, D. Huh, C. R. Kyrtsos, T. Houssin, N. Futai, and S. Takayama, *Analytical chemistry,* 2007, **79**(9), 3504.
45 M. Noris, M. Morigi, R. Donadelli, S. Aiello, M. Foppolo, M. Todeschini, S. Orisio, G. Remuzzi, and A. Remuzzi, *Circulation research,* 1995, **76**(4), 536.
46 J. Seebach, P. Dieterich, F. Luo, H. Schillers, D. Vestweber, H. Oberleithner, H. J. Galla, and H. J. Schnittler, *Lab Invest,* 2000, **80**(12), 1819.
47 O. C. Colgan, G. Ferguson, N. T. Collins, R. P. Murphy, G. Meade, P. A. Cahill, and P. M. Cummins, *Am J Physiol Heart Circ Physiol,* 2007, **292**(6), H3190.
48 M. Rossi, R. Lindken, B. P. Hierck, and J. Westerweel, *Lab Chip,* 2009, **9**(10), 1403.
49 J. Wang, J. Heo, and S. Z. Hua, *Lab Chip,* 2010, **10**(2), 235.
50 L. Wang, Z. L. Zhang, J. Wdzieczak-Bakala, D. W. Pang, J. Liu, and Y. Chen, *Lab Chip,* 2011, **11**(24), 4235.
51 S. Y. Desai, M. Marroni, L. Cucullo, L. Krizanac-Bengez, M. R. Mayberg, M. T. Hossain, G. G. Grant, and D. Janigro, *Endothelium,* 2002, **9**(2), 89.
52 K. Aran, L. A. Sasso, N. Kamdar, and J. D. Zahn, *Lab Chip,* 2010, **10**(5), 548.
53 B. H. Chueh, D. Huh, C. R. Kyrtsos, T. Houssin, N. Futai, and S. Takayama, *Anal Chem,* 2007, **79**(9), 3504.
54 J. T. Kuo, L.-Y. Chang, P.-Y. Li, T. Hoang, and E. Meng, *Sensors and Actuators B: Chemical,* 2011, **152**(2), 267.
55 Y. Omidi, L. Campbell, J. Barar, D. Connell, S. Akhtar, and M. Gumbleton, *Brain Res,* 2003, **990**(1-2), 95.
56 F. M. White, *Fluid Mechanics*. 4 ed. 1999: McGraw-Hill International.
57 I. Papautsky, B. K. Gale, S. Mohanty, T. A. Ameel, and A. B. Frazier, *Proceedings of SPIE-The International Society for Optical Engineering, Proceedings of the 1999 Microfluidic Devices and Systems II, Santa Clara,* 1999, **3877**(147.
58 T. Gervais, J. El-Ali, A. Gunther, and K. F. Jensen, *Lab Chip,* 2006, **6**(4), 500.
59 W. Yuan, G. Li, E. S. Gil, T. L. Lowe, and B. M. Fu, *Ann Biomed Eng,* 2010, **38**(4), 1463.
60 W. M. Pardridge, D. Triguero, J. Yang, and P. A. Cancilla, *J Pharmacol Exp Ther,* 1990, **253**(2), 884.
61 G. Li, M. J. Simon, L. M. Cancel, Z. D. Shi, X. Ji, J. M. Tarbell, B. Morrison, 3rd, and B. M. Fu, *Ann Biomed Eng,* 2010, **38**(8), 2499.
62 T. Maciag, J. Kadish, L. Wilkins, M. B. Stemerman, and R. Weinstein, *The Journal of Cell Biology,* 1982, **94**(3), 511.
63 M. Vastag and G. M. Keseru, *Curr Opin Drug Discov Devel,* 2009, **12**(1), 115.

